Science of the Total Environment 858 (2023) 159951

Contents lists available at ScienceDirect

Science of the Total Environment

journal homepage: www.elsevier.com/locate/scitotenv

# Two-year online measurements of volatile organic compounds (VOCs) at four sites in a Chinese city: Significant impact of petrochemical industry

Jiangshan Mu [a], Yingnan Zhang [a,*], Zhiyong Xia [b], Guolan Fan [b], Min Zhao [a], Xiaoyan Sun [b], Yuhong Liu [c], Tianshu Chen [a], Hengqing Shen [a], Zhanchao Zhang [b], Huaicheng Zhang [b], Guang Pan [b], Wenxing Wang [a], Likun Xue [a,b,**]

[a] Environment Research Institute, Shandong University, Qingdao, Shandong 266237, China
[b] Ji'nan Ecological Environment Monitoring Center of Shandong Province, Ji'nan, Shandong 250000, China
[c] Key Laboratory of Marine Environment and Ecology, Frontiers Science Center for Deep Ocean Multispheres and Earth System, Ministry of Education, Ocean University of China, Qingdao, Shandong 266100, China

## HIGHLIGHTS

- Two-year online measurements of VOCs were conducted at four sites in a Chinese city.
- Petrochemical industry led to higher VOC level and larger aromatic contribution.
- Strong $O_3$ production and high sensitivity to $NO_x$ were determined at industrial site.

## GRAPHICAL ABSTRACT

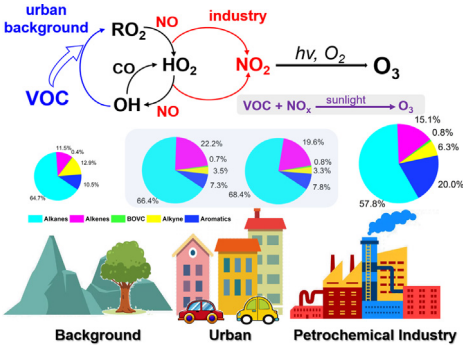


## ARTICLE INFO

Editor: Hai Guo

*Keywords:*
Volatile organic compounds
Spatio-temporal distribution
Petrochemical industry
Observation-based model
Ozone

## ABSTRACT

Volatile organic compounds (VOCs) management has been recently given a high priority in China to mitigate ozone ($O_3$) air pollution. However, there is a relatively poor understanding of VOCs due to their complexity and fewer observations. To better understand the pollution characteristics of VOCs and their impact on $O_3$ pollution, two-year continuous measurements were conducted at four representative sites in Ji'nan, eastern China. These four sites cover urban, background, and industrial areas (within a petroleum refinery). Ambient VOCs showed higher concentrations at industrial site than at urban and background sites, owing to intensive emissions from petrochemical industry. The VOCs compositions present spatial heterogeneity with alkenes dominated in total reactivity at urban and background sites, while alkenes and aromatics together dominated at industrial site. The VOCs emission profile from petrochemical industry was calculated based on observational data, which revealed a huge impact on light alkanes ($C_2$–$C_5$), light alkenes (ethene), and aromatics (toluene and *m/p*-xylene). The positive matrix factorization (PMF) model analysis further refined the impact of different petrochemical industrial processes. Alkanes and alkenes dominated the emissions during refining process, while aromatics dominated during solvent usage process. Analysis by an observation-based model indicated stronger in-situ $O_3$ production and higher sensitivity to nitrogen oxides at industrial site compared to urban and background sites. The reduction of VOCs emissions from petrochemical

* Corresponding author.
** Correspondence to: L. Xue, Environment Research Institute, Shandong University, Qingdao, Shandong 266237, China.
*E-mail addresses:* yingnan@mail.sdu.edu.cn (Y. Zhang), xuelikun@sdu.edu.cn (L. Xue).

http://dx.doi.org/10.1016/j.scitotenv.2022.159951
Received 14 August 2022; Received in revised form 24 October 2022; Accepted 31 October 2022
Available online 3 November 2022

industry would significantly reduce the $O_3$ concentrations. The analyses underline the significant impact of petrochemical industry on VOCs and $O_3$ pollution, and provide important reference for the formulation of refined and effective control strategies.

## 1. Introduction

Volatile organic compounds (VOCs) and nitrogen oxides ($NO_x$ = NO + $NO_2$) are key precursors to the formation of secondary aerosols and ground-level ozone ($O_3$), and hence play important roles in tropospheric chemistry and regional air quality (Atkinson, 2000; Liu et al., 2019; Seinfeld and Pandis, 1998; Sillman, 1999; Wu et al., 2016). Scores of studies have demonstrated significant decreases in the emissions and ambient concentrations of $NO_x$ across China in the recent decade, owing to the implementation of a series of regulations launched by the China State Council (Wang et al., 2019; Wang et al., 2022). In comparison, little attention has been paid to VOCs control, which still exhibited an increasing or non-decreasing trend (Li et al., 2019a, 2019b; Wu and Xie, 2017), and thereby largely contributed to the worsened secondary air pollution problems (especially $O_3$ air pollution) in China (Sun et al., 2016; Xue et al., 2014).

Extensive studies have been conducted to examine the VOCs pollution characteristics, sources, and impact on $O_3$ pollution over the last three decades. Most studies have been concentrated in fast-developing regions, such as Beijing-Tianjin-Hebei and surrounding areas (BTHs), Yangtze River Delta (YRD), and Pearl River Delta. High levels of ambient VOCs and a VOCs-limited $O_3$ formation regime have been frequently documented in Beijing, Shanghai, Guangzhou, and Hong Kong (Guo et al., 2017; Wang et al., 2017; Mozaffar and Zhang, 2020; Xue et al., 2014), elucidating the importance of VOCs to chemical production of $O_3$ in the metropolitan areas. Vehicle exhaust and industrial activity were identified as major emission sectors for VOCs based on source apportionment results (Dai et al., 2022; Guo et al., 2017; Li et al., 2020a, 2020b; Li et al., 2019a, 2019b). Despite an increasing number of studies, the current observations are not sufficiently comprehensive to reflect the VOCs pollution situation in China. First, most studies were based on short-term intensive observations, while long-term measurements of VOCs with >1-year period are very limited. Second, many other cities beyond metropolitan areas are also facing serious VOCs and $O_3$ air pollution problems, but limited studies were taken place.

Shandong Province is located in East China and behaves as a connection for BTHs and the YRD region. This area is densely-populated and suffered from heavy traffic and residential emissions. In addition, it has a solid foundation and booming development of industry, e.g., the output in the fields of petroleum refinery industry of Shandong was in the front rank over China and worldwide. The flourishing petroleum refinery industry has enormously promoted the economic development over Shandong, but also led to large energy consumption and deterioration of air quality. A variety of VOCs species would be emitted into the atmosphere from crude oil volatilization, refining process, and solvent usage during the petrochemical industrial process (Chen et al., 2020; Rao et al., 2007), which would subsequently contribute to the chemical production of $O_3$. Indeed, the environmental impact of petrochemical industry goes far beyond Shandong Province, as which is an important industrial source for VOCs emissions in China and many other countries (Han et al., 2018; Rovira et al., 2021). A comprehensive understanding of the impact of petrochemical industry on VOCs and $O_3$ air pollution is therefore essential for the formulation of efficient and refined control strategies.

Ji'nan is the capital city of Shandong Province and is home to several large petroleum refineries. In this study, we conducted 2-year continuous observations at urban, background, and industrial sites of Ji'nan during 2018–2019. The obtained data were analyzed in detail to examine the tempo-spatial distributions of VOCs as well as the impact of petrochemical industry on VOCs abundance and chemical compositions. The emission profile of VOCs from petrochemical industry and its major processes is determined based on observational data and positive matrix factorization (PMF) model analysis. The $O_3$ formation mechanism and the impact of major emission sources on $O_3$ formation at individual sites are determined with the application of an observation-based model (OBM). The implications for the formulation of control strategies against $O_3$ pollution is discussed.

## 2. Materials and methods

### 2.1. Site description and field observations

Four sites distributed in three functional areas (i.e., urban, background, and industrial areas) of Ji'nan were carefully selected for field observations. The locations of individual sites are shown in Fig. 1 and the detailed descriptions are as follows.

Two urban sites were selected, with one located in Quancheng Square (QS; 36.66°N, 117.02°E; 35 m above sea level (a.s.l.)), and the other located in Environmental Monitoring Center Station (EMCS; 36.66°N, 117.15°E; 35 m a.s.l.). These two sites are very close and both are located in the prosperous area of central Ji'nan, with residential areas, commercial areas, and arterial roads nearby. In addition, a petroleum refinery (where the industrial site is located) is located about ~15 km to the northeast. The air quality in urban Ji'nan is mainly affected by anthropogenic emissions, especially vehicle exhaust and industrial activity (to a lesser extent). The observations lasted from 2 March 2018 to 31 December 2019 at QS and from 8 January 2018 to 31 December 2019 at EMCS.

The industrial site was set in a petroleum refinery company (OR; 36.70°N, 117.17°E; 16 m a.s.l.), which covers an area of ~2400 $m^2$ and is located in the central part of Ji'nan (close to the urban areas). The OR company belongs to a large Chinese petroleum and chemical company and can produce ~5 million tons of oils annually. In addition to the significant impact from industrial activity, the OR site is somewhat affected by vehicle exhaust as the company is close to an arterial road. The observations lasted from 7 January 2018 to 31 December 2019.

The background site is located in Paomaling park (PML; 36.43°N, 117.22°E; 710 m a.s.l.) in a mountainous area in southern Ji'nan, which is ~40 km far away from the urban sites and ~50 km far away from the industrial site. The mountains have an average elevation of ~700 m a.s.l. Due to the high elevation, the PML site is rarely impacted by local anthropogenic emissions. The observations lasted from 6 January 2018 to 31 December 31, 2019.

The VOCs data were measured with TH-300B Online VOCs Monitoring System made by *Wuhan Tianhong Environmental Protection Industry Co., Ltd.* This system adopted detection technology of ultra-low temperature preconcentration combined with gas chromatography and mass spectrometry-flame ionization detector (GC/MS-FID). The ultra-low temperature freeze recovery device uses electronic refrigeration, and the internal temperature of the cold trap can reach −150 °C, allowing the target compound to be completely captured. During the sampling period, strict quality assurance and control procedures were performed to assure data quality (MEEPRC, 2013). Briefly, single-point calibrations and multi-point calibrations were regularly performed on a weekly basis by using the standard gases of PAMS and TO15. The $R^2$ of the calibration curves for all compounds was >0.995. The method detection limit (MDL) for species quantified in this system ranged from 0.001 to 0.040 ppbv (the statistical confidence coefficient was 3.14), which was determined by repeating the analysis 7 times with standard sample at a concentration of the lowest calibration curve. The accuracy of individual species was within ±9 %, which was determined by comparison between measured values and actual values with weekly span checks and calibrations. The precision of individual species was within 10 %, which was determined by repeating the analysis 5 times with standard sample at a concentration of 2 ppbv. Previous studies

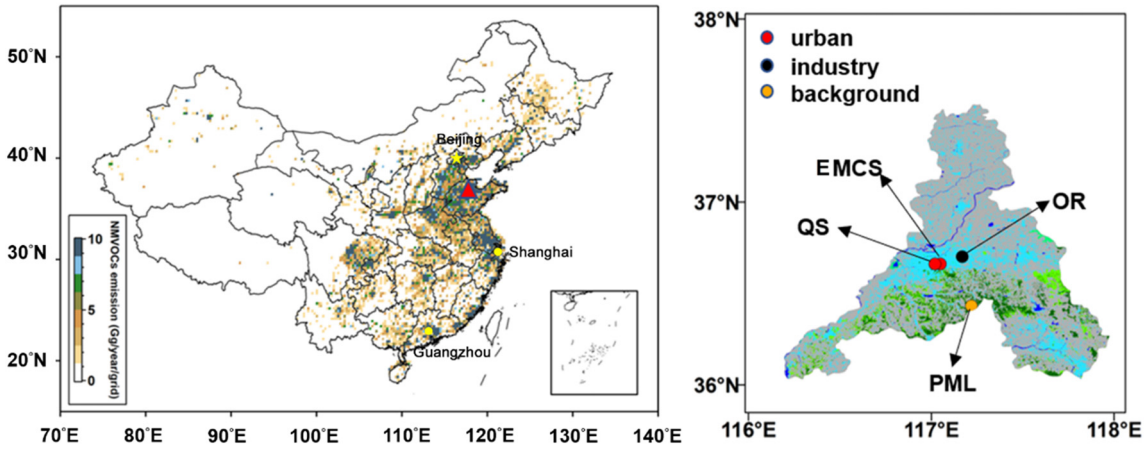


**Fig. 1.** Map showing the location of Ji'nan (the red triangle in the left panel) and the distributions of four observation sites within Ji'nan (the right panel). The left panel was colored by NMVOC emissions in 2016 (Li et al., 2017), while the right panel was colored by land-use types, and the grey, cyan, and green colors were used to represent cropland, artificial surface, and forest land, respectively. NMVOC, non-methane volatile organic compound; QS, Quancheng square; EMCS, Environmental Monitoring Center Station; OR, petroleum refinery company; PML, Paomaling park.

have confirmed the satisfactory ability of TH-300B for VOCs detection and analysis (Wang et al., 2014). In this study, totally 57 VOCs species (see Table 1 for detailed information) were the same within observations at four sites, and their data were extracted for further analyses.

Observational data for trace gases and meteorological parameters were obtained from local government agencies. Trace gases including CO, $O_3$, $SO_2$, and $NO_2$ were measured with standard commercial techniques (CNEMC, 2018). Specifically, $O_3$ was measured by a model T400 UV photometric ozone analyzer (Teledyne Advanced Pollution Instrumentation (T-API)) with a detection limit of 0.4 ppbv and precision of 0.5 %. $NO_2$ was monitored by an optical analyzer (model T500U, T-API) with a detection limit of 40 pptv and precision of 0.5 %. CO was measured using a model 300 optical analyzer (T-API) with a detection limit of 50 ppbv and precision of 0.5 %. $SO_2$ was measured by the model T100U trace-level analyzer with a detection limit of 0.4 ppbv and precision of 0.5 %. During the 2-yr observation, multi-point calibrations were performed monthly and zero and span calibrations were performed weekly. The measured meteorological parameters include wind speed, wind direction, temperature, relative humidity, and barometric pressure.

### 2.2. The PMF model

The PMF method is an effective multivariate factor analysis tool and has been widely used to resolve VOCs sources. Briefly, PMF would decompose the sampled data into two matrices: factor contributions and factor profiles. These factor profiles can be interpreted to explore source types and contributions (Paatero, 1997; Paatero and Tapper, 1994). In this study, the US PMF 5.0 (EPA, 2014) was applied to identify major VOCs sources and to estimate their contributions to VOCs observed at individual sites. Compounds with data caption rate below 75 % were rejected. Finally, the data of total 40, 32, and 44 VOCs species which are representative tracers of specific sources were selected as input to the PMF model for urban, industrial, and background sites, respectively. These selected species accounted for a large contribution to the total concentration and OH reactivity of VOCs species, i.e., 93.4 % and 80.4 % at urban sites, 82.9 % and 82.1 % at industrial site, and 96.0 % and 83.3 % at background site, and are supposed to be able to reflect the local emission characteristics. The uncertainty is estimated according to Eq. (1) and Eq. (2) (EPA, 2014).

$$uncertainly = \frac{5}{6} \times MDL(C \le MDL) \quad (1)$$

$$uncertainty = \sqrt{(EF \times concentration)^2 + (0.5 \times MDL)^2}(C > MDL) \quad (2)$$

where MDL represents method detection limit; C represents the concentration of each selected species; EF represents error fraction, and was assumed to be 20 % in this study.

A series of PMF runs were performed to find a reasonable number of identified sources (six for industrial and urban sites; five for background site) and to ensure that the theoretical Q value is closer to or approximately equal to the number of freedom degrees or the total number of data points. The detailed criteria for factor selection and identification have been provided in previous studies (An et al., 2017; Liu et al., 2020).

### 2.3. Chemical box model

An observation-based model was used to estimate the in-situ $O_3$ production rates and to diagnose the $O_3$ formation mechanisms at the individual sites. The OBM is built based on the Regional Atmospheric Chemical Mechanism version 2 (RACM2) (Gross and Stockwell, 2003; Stockwell et al., 1997) and incorporates physical processes such as dry deposition and diurnal variation of planetary boundary layer (see SI for the descriptions). Detailed information of model configuration and performance can be found in previous studies (Liu et al., 2021b; Zong et al., 2018).

We performed OBM simulations for spring, summer, and autumn, three of the photochemically-active seasons (see the frequency of maximum daily 8-hour average $O_3$ (MDA8 $O_3$) mixing ratio exceeding 75 ppbv (Class II standard in China) in Fig. S1). During the simulations, the OBM was constrained by the observed data of $O_3$, CO, $SO_2$, $NO_2$ and VOCs (57 compounds) concentrations, and meteorological parameters (e.g., temperature, relative humidity, and pressure), which were averaged or interpolated into a 30-min resolution. The data of *m*-xylene and *p*-xylene cannot be separately measured, and were regarded as *m*-xylene in the model input. The model was initiated at 00:00 local time (LT) and read the input data at an integration step of 30 min to calculate in-situ $O_x$ ($O_x = O_3 + NO_2$) production, destruction, and net rates during the entire spring, summer, and autumn seasons of 2018 and 2019. Prior to each simulation, the model was pre-run for 3 days to approach a steady state to stabilize the concentrations of unconstrained species (such as radicals and oxygenated VOCs (OVOCs)), and results from the 4th day were extracted for analyses. A series of sensitivity tests were conducted to evaluate the effects of $NO_x$ and VOCs (including anthropogenic VOCs (AVOCs) and biogenic VOCs (BVOCs), and AVOCs were further divided into alkanes, alkenes, and aromatics) and of major VOCs emission sources (identified by PMF model) on the net rates of in-situ $O_x$ production.

Ozone isopleth diagrams were established to describe the non-linear relationship between $O_3$ and its precursors (i.e., $NO_x$ and AVOCs) at industrial and urban sites. Briefly, the RACM2 box model was constrained in the base run by the average diurnal profile of $SO_2$, CO, $NO_2$ and VOCs

**Table 1**
The average mixing ratio (mean ± standard deviation; unit: ppbv) of VOCs observed at four sites in Ji'nan during 2018–2019.

| Species | QS | EMCS | OR | PML |
|---|---|---|---|---|
| Ethane | 3.63 ± 1.62 | 3.27 ± 1.67 | 5.00 ± 2.92 | 2.62 ± 1.58 |
| Propane | 3.65 ± 2.43 | 3.80 ± 2.64 | 4.75 ± 3.32 | 1.03 ± 0.65 |
| *n*-Butane | 2.32 ± 1.71 | 1.78 ± 1.44 | 2.98 ± 2.70 | 0.57 ± 0.36 |
| *i*-Butane | 0.61 ± 0.52 | 0.78 ± 0.61 | 2.25 ± 2.17 | 0.43 ± 0.24 |
| Cyclopentane | 0.05 ± 0.03 | 0.06 ± 0.05 | 0.45 ± 1.13 | 0.02 ± 0.02 |
| *n*-Pentane | 0.32 ± 0.29 | 0.49 ± 0.46 | 2.01 ± 2.35 | 0.20 ± 0.14 |
| *i*-Pentane | 0.91 ± 0.70 | 1.30 ± 1.02 | 2.85 ± 2.72 | 0.28 ± 0.18 |
| Cyclohexane | 0.06 ± 0.05 | 0.04 ± 0.03 | 0.26 ± 0.49 | 0.02 ± 0.02 |
| Methylcyclopentane | 0.06 ± 0.04 | 0.07 ± 0.05 | 0.49 ± 0.98 | 0.02 ± 0.02 |
| 2,3-Dimethylbutane | 0.20 ± 0.15 | 0.21 ± 0.17 | 0.77 ± 1.29 | 0.03 ± 0.03 |
| 2,2-Dimethylbutane | 0.03 ± 0.02 | 0.03 ± 0.02 | 0.12 ± 0.32 | 0.01 ± 0.01 |
| *n*-Hexane | 0.04 ± 0.04 | 0.04 ± 0.04 | 0.92 ± 1.29 | 0.05 ± 0.04 |
| 2-Methylpentane | 0.25 ± 0.16 | 0.28 ± 0.19 | 0.63 ± 1.08 | 0.03 ± 0.03 |
| 3-Methylpentane | 0.10 ± 0.07 | 0.13 ± 0.10 | 0.65 ± 1.14 | 0.03 ± 0.03 |
| Methylcyclohexane | 0.04 ± 0.03 | 0.04 ± 0.03 | 0.26 ± 0.48 | 0.01 ± 0.01 |
| *n*-Heptane | 0.06 ± 0.04 | 0.05 ± 0.04 | 0.55 ± 0.72 | 0.05 ± 0.04 |
| 2-Methylhexane | 0.04 ± 0.04 | 0.05 ± 0.04 | 0.29 ± 0.56 | 0.01 ± 0.01 |
| 2,3-Dimethylpentane | 0.03 ± 0.02 | 0.02 ± 0.02 | 0.21 ± 0.41 | 0.01 ± 0.01 |
| 2,4-Dimethylpentane | 0.02 ± 0.01 | 0.02 ± 0.01 | 0.10 ± 0.20 | 0.01 ± 0.01 |
| 3-Methylhexane | 0.05 ± 0.04 | 0.05 ± 0.04 | 0.33 ± 0.58 | 0.01 ± 0.01 |
| *n*-Octane | 0.03 ± 0.02 | 0.03 ± 0.03 | 0.32 ± 0.47 | 0.02 ± 0.02 |
| 2,3,4-Trimethylpentane | 0.02 ± 0.01 | 0.02 ± 0.01 | 0.08 ± 0.15 | 0.01 ± 0.01 |
| 2-Methylheptane | 0.02 ± 0.01 | 0.02 ± 0.01 | 0.21 ± 0.41 | 0.01 ± 0.01 |
| 3-Methylheptane | 0.02 ± 0.01 | 0.02 ± 0.01 | 0.15 ± 0.25 | 0.01 ± 0.01 |
| 2,2,4-Trimethylpentane | 0.03 ± 0.02 | 0.03 ± 0.02 | 0.15 ± 0.33 | 0.01 ± 0.01 |
| *n*-Nonane | 0.03 ± 0.02 | 0.02 ± 0.02 | 0.40 ± 0.54 | 0.02 ± 0.02 |
| *n*-Decane | 0.02 ± 0.01 | 0.02 ± 0.01 | 0.55 ± 0.91 | 0.04 ± 0.06 |
| *n*-Undecane | 0.02 ± 0.01 | 0.02 ± 0.01 | 0.43 ± 0.62 | 0.10 ± 0.18 |
| *n*-Dodecane | 0.03 ± 0.02 | 0.03 ± 0.02 | 0.27 ± 0.52 | 0.05 ± 0.03 |
| Ethene | 1.47 ± 1.01 | 1.38 ± 1.04 | 2.88 ± 2.55 | 0.74 ± 0.62 |
| Propene | 0.72 ± 0.74 | 0.74 ± 0.83 | 1.61 ± 3.06 | 0.20 ± 0.23 |
| 1,3-Butadiene | 0.11 ± 0.09 | 0.08 ± 0.05 | 0.13 ± 0.34 | 0.00 ± 0.00 |
| 1-Butene | 1.25 ± 0.93 | 0.73 ± 0.56 | 0.54 ± 1.17 | 0.04 ± 0.03 |
| *Cis*-2-butene | 0.24 ± 0.12 | 0.22 ± 0.12 | 0.33 ± 0.76 | 0.04 ± 0.03 |
| *Trans*-2-butene | 0.08 ± 0.08 | 0.09 ± 0.07 | 0.50 ± 1.22 | 0.05 ± 0.06 |
| 1-Pentene | 0.13 ± 0.10 | 0.16 ± 0.12 | 0.30 ± 0.85 | 0.02 ± 0.02 |
| *Cis*-2-pentene | 0.03 ± 0.02 | 0.05 ± 0.05 | 0.19 ± 0.62 | 0.00 ± 0.00 |
| *Trans*-2-pentene | 0.10 ± 0.07 | 0.13 ± 0.10 | 0.52 ± 1.14 | 0.03 ± 0.03 |
| 1-Hexene | 0.04 ± 0.03 | 0.04 ± 0.03 | 0.29 ± 0.61 | 0.04 ± 0.04 |
| Isoprene | 0.12 ± 0.12 | 0.14 ± 0.14 | 0.38 ± 0.82 | 0.03 ± 0.04 |
| Ethyne | 0.61 ± 0.42 | 0.57 ± 0.42 | 2.85 ± 2.32 | 0.99 ± 0.63 |
| Benzene | 0.58 ± 0.37 | 0.59 ± 0.40 | 1.35 ± 1.32 | 0.33 ± 0.20 |
| Toluene | 0.34 ± 0.26 | 0.36 ± 0.31 | 1.46 ± 1.34 | 0.20 ± 0.19 |
| Styrene | 0.04 ± 0.03 | 0.03 ± 0.03 | 0.20 ± 0.34 | 0.01 ± 0.01 |
| Ethylbenzene | 0.09 ± 0.08 | 0.09 ± 0.08 | 0.55 ± 0.62 | 0.05 ± 0.05 |
| *o*-Xylene | 0.09 ± 0.08 | 0.09 ± 0.09 | 0.63 ± 0.68 | 0.05 ± 0.05 |
| *m/p*-Xylene | 0.16 ± 0.15 | 0.18 ± 0.18 | 1.51 ± 1.57 | 0.09 ± 0.08 |
| *n*-Propylbenzene | 0.02 ± 0.01 | 0.02 ± 0.01 | 0.27 ± 0.43 | 0.02 ± 0.02 |
| Isopropylbenzene | 0.01 ± 0.01 | 0.01 ± 0.01 | 0.12 ± 0.22 | 0.01 ± 0.01 |
| *p*-Ethyltoluene | 0.02 ± 0.02 | 0.03 ± 0.02 | 0.36 ± 0.52 | 0.02 ± 0.02 |
| *o*-Ethyltoluene | 0.02 ± 0.01 | 0.02 ± 0.01 | 0.35 ± 0.50 | 0.02 ± 0.02 |
| 1,2,4-Trimethylbenzene | 0.04 ± 0.04 | 0.04 ± 0.04 | 0.77 ± 1.11 | 0.03 ± 0.03 |
| 1,3,5-Trimethylbenzene | 0.04 ± 0.03 | 0.04 ± 0.03 | 0.37 ± 0.54 | 0.01 ± 0.01 |
| 1,2,3-Trimethylbenzene | 0.02 ± 0.02 | 0.02 ± 0.02 | 0.43 ± 0.74 | 0.02 ± 0.02 |
| *p*-Diethylbenzene | 0.02 ± 0.01 | 0.02 ± 0.02 | 0.45 ± 0.84 | 0.04 ± 0.08 |
| *m*-Diethylbenzene | 0.02 ± 0.01 | 0.02 ± 0.01 | 0.39 ± 0.71 | 0.02 ± 0.04 |

concentrations, temperature, relative humidity, and pressure during $O_3$ non-attainment days (i.e., MDA8 $O_3$ mixing ratios were higher than the Chinese Class II standard of 75 ppbv). These average diurnal profiles of major pollutants and meteorological parameters have a good representativeness of the local environmental conditions facilitating $O_3$ pollution (Fig. S2–S3). Then, a series of emission-reduction simulations were conducted using $X$ times ($X$ = 0–1, with a bin of 0.05) the base concentrations of AVOCs and $NO_x$. For more reliable modeling results, the initial concentrations of OVOCs were specified based on 2-day pre-run results. The concentration of $O_3$ was initialized using observation data at 00:00 local time (LT) (initial time of the model integration), and its chemistry and concentration were simulated using constraints for other relevant species in the following integration. The model was initialized at 00:00 LT with an integration step of 1 h and a duration of 24 h. The model-simulated MDA8 $O_3$ concentrations under the above base and 399 emission-reduction scenarios were extracted to describe the nonlinear response of $O_3$ to reduction in $O_3$ precursors.

## 3. Results and discussion

### 3.1. Chemical composition and spatial distribution of ambient VOCs

Table 1 presents and compares the average VOCs concentrations observed at urban, background, and industrial sites. The average VOCs concentrations (± standard deviation) were 45.2 ± 28.4 ppbv at industrial site, significantly higher than those at urban sites (17.6 ± 8.1 ppbv at QS; 17.1 ± 8.4 ppbv at EMCS) and background site (7.7 ± 3.7 ppbv) ($p < 0.01$, tested by one-way analysis of variance). This is also the case from the perspective of reactivity, with the highest OH reactivity ($L_{OH}$) recorded at industrial site (7.3 ± 4.3 $s^{-1}$), followed by urban sites (3.9 ± 1.9 $s^{-1}$ at QS; 3.6 ± 1.8 $s^{-1}$ at EMCS) and background site (0.9 ± 0.5 $s^{-1}$) ($p < 0.01$). Such spatial distribution pattern is common for most species, with one exception of 1-butene, which showed the highest concentrations at urban sites, and then followed by industrial site and background site. The distinct spatial distribution pattern of 1-butene was indeed attributed to the intense oil and gas usage emissions in urban areas (similar case was also observed in Beijing (Cui et al., 2022)), which is a major source of 1-butene. We then compared the VOCs abundance in Ji'nan with that in other cities. As shown in Fig. S4, the VOCs concentrations in urban Ji'nan were lower than those observed in London (Von Schneidemesser et al., 2010), Los Angeles (Warneke et al., 2012), and Tokyo (Hoshi et al., 2008), and ranked at middle levels among the selected 17 Chinese cities. However, the VOCs concentrations at the industrial site were comparable to or higher than those observed in the above selected cities. Furthermore, the VOCs concentrations at industrial site in the present study was comparable with those observed at other industrial sites with intense VOCs emission (An et al., 2014; Wang et al., 2021; Wei et al., 2022). These results demonstrate the intensive VOCs emission from petrochemical industry.

The detailed VOCs compositions also varied spatially (Fig. 2). With concentration-based results, alkanes made the largest contributions (OR: 57.8 %; QS: 66.4 %; EMCS: 68.4 %; PML: 64.7 %). The second abundant class was aromatics at industrial site, but changed to alkenes and alkynes at urban sites (QS: 22.2 %; EMCS: 19.6 %) and background site (12.9 %), respectively. It appears that petrochemical industry would lead to higher aromatic contributions (particularly of toluene and *m/p*-xylene), which is more obvious with $L_{OH}$-based results. As shown, alkenes were the key class at urban and background sites (QS: 69.0 %; EMCS: 64.0 %; PML: 44.0 %), whose contributions to $L_{OH}$ were obviously higher than the other classes. On species level, 1-butene and ethene made the largest contributions at urban sites (QS: 23.9 %, 1.05 ± 0.79 $s^{-1}$; EMCS: 15.3 %, 0.62 ± 0.47 $s^{-1}$) and background site (14.0 %, 0.17 ± 0.14 $s^{-1}$), respectively. In contrast, alkenes and aromatics made comparable contributions (37.6 % vs 35.7 %) and together dominated $L_{OH}$ at industrial site. On species level, propene (12.9 %, 1.06 ± 2.00 $s^{-1}$) and *m/p*-xylene (9.5 %, 0.78 ± 0.64 $s^{-1}$) made the largest contributions. In addition, we notice that the contributions of unreactive species (e.g., alkynes and alkanes) were higher at background sites than at urban and industrial sites, indicating a nature of regional transport. These results clearly elucidate the varied VOCs chemical composition among different sites in Ji'nan.

The spatial distribution pattern of VOCs and its chemical composition reflected the distinct emission characteristics among different functional areas in a particular city. For Ji'nan, the VOCs at urban and background sites were mainly subject to the influence of oil and gas usage and combustion source (both with large loads of alkenes), respectively, while at industrial site were mainly subject to the influence of petrochemical industrial emission (with large loads of aromatics) (see details in Section 3.3). The spatial distribution pattern of VOCs in Ji'nan reveals the intensive VOCs (especially aromatics) emission from petrochemical industry activity.

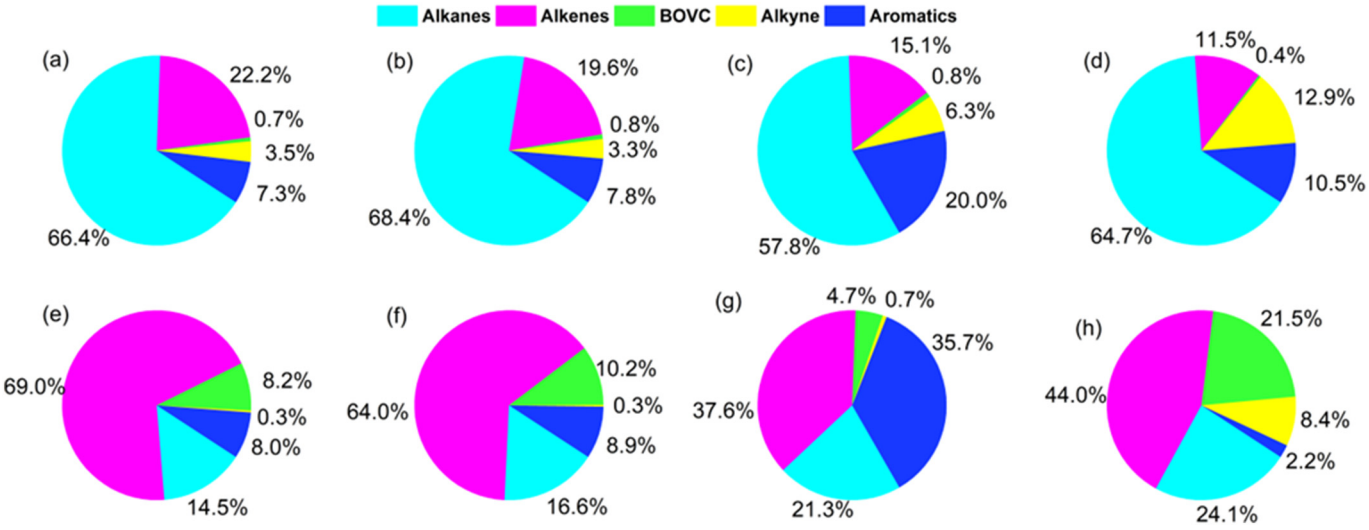


**Fig. 2.** VOCs compositions based on concentrations (the upper panel) and $L_{OH}$ (the lower panel) at QS ((a) and (e)), EMCS ((b) and (f)), OR ((c) and (g)), and PML ((d) and (h)) in Ji'nan.

### 3.2. Seasonal and diurnal variations

Fig. 3 depicts the seasonal variation pattern of VOCs concentrations derived from the 2-year continuous observations. At urban and industrial sites, the VOCs concentrations were the lowest in spring (March–May; 14.0 ± 7.3 ppbv at QS, 14.0 ± 7.5 ppbv at EMCS, and 31.5 ± 21.2 ppbv at OR) and peaked in autumn (September–November; 20.9 ± 8.6 ppbv at EMCS) or winter (December–January; 20.4 ± 7.4 ppbv at QS; 56.1 ± 28.4 ppbv at OR). Such pattern is typical for cities located in northern China, e.g., Beijing (Liu et al., 2021a), Shijiazhuang (Guan et al., 2020), and Taiyuan (Li et al., 2020a, 2020b), and should be attributed to the favorable meteorological conditions in spring (e.g., high planetary boundary layer) and unfavorable meteorological conditions (e.g., shallow planetary boundary layer) and strong emission intensity (from heat and burning, etc.) in autumn and winter. A similar pattern was also shown by individual AVOCs group (Fig. S5), while BVOCs (i.e., isoprene) concentrations peaked in summer due to high temperatures. At background site, the VOCs concentrations exhibited a valley in summer (June–August; 6.2 ± 2.6 ppbv) and peaked in winter (9.8 ± 4.8 ppbv). For comparison, we also performed similar analyses based on $L_{OH}$ (Fig. 3), and the obtained results are generally consistent with those obtained based on VOCs concentrations.

Fig. 4 presents the average diurnal variation pattern of VOCs concentrations at individual sites. At urban and industrial sites, the VOCs concentrations showed well-defined diurnal pattern with two peaks in the morning and early evening rush hours. A similar pattern was shown by $NO_2$ concentrations (Fig. S6). Such pattern is typical for most of the existing studies conducted in urban areas and highlights the significant impact of vehicle exhaust and planetary boundary layer evolution (Fares et al., 2013; Li

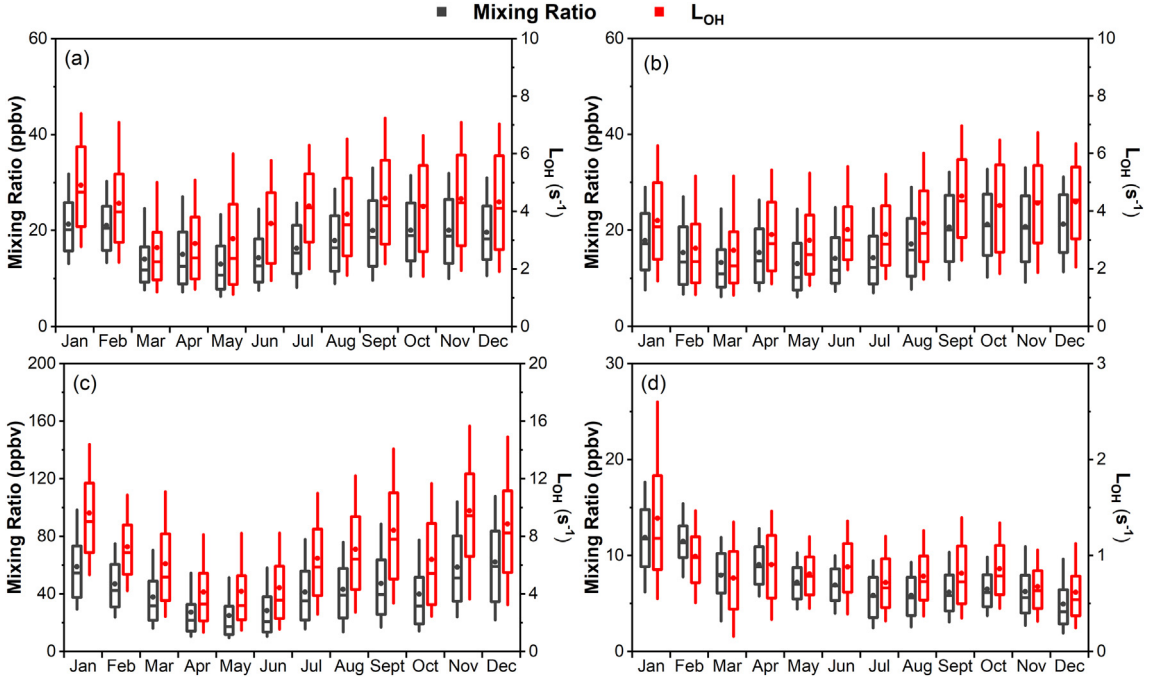


**Fig. 3.** Seasonal variations of ambient VOCs at (a) QS, (b) EMCS, (c) OR, and (d) PML in Ji'nan during 2018–2019. The box plot provides the 10 %, 25 %, 50 %, 75 %, and 90 % of the data, while the dots indicate the average concentrations.

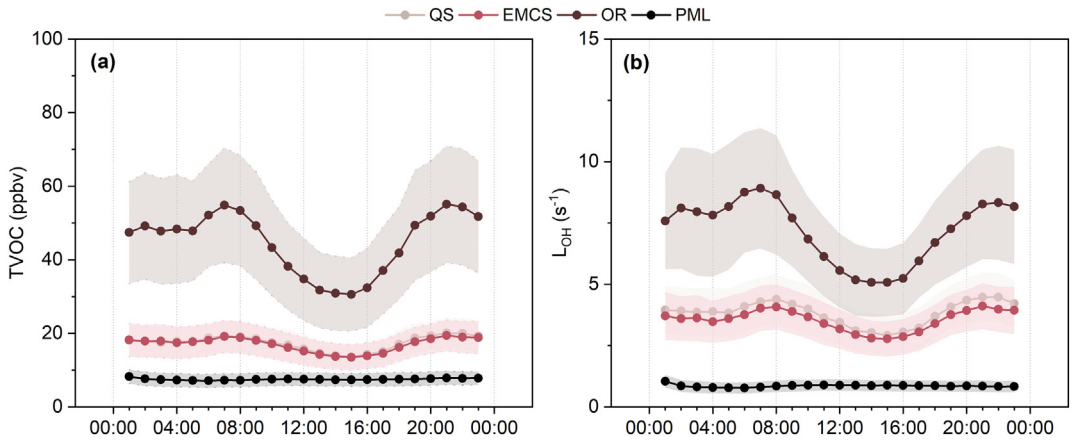


**Fig. 4.** Average diurnal variations in (a) concentrations and (b) $L_{OH}$ of ambient VOCs at individual sites in Ji'nan during 2018–2019. The shaded areas represent half standard deviation of the mean.

et al., 2014; Liu et al., 2016). All of the AVOCs groups (such as alkanes, alkenes, and aromatics) showed a bi-modal diurnal variation pattern, while BVOCs exhibited a broad peak in the afternoon due to high temperatures (Fig. S7). At background site, the diurnal pattern of VOCs concentrations was very flat with much smaller variations than those observed at urban and industrial sites. A similar pattern was shown by $NO_2$ concentrations (Fig. S6). Such pattern is typical for most of the existing studies conducted in remote areas (Debevec et al., 2021), implying the influence of regional transport.

The above temporal distribution pattern of VOCs is shaped by a combination of many factors, including emission intensity, sinks, regional transport, and meteorological conditions. The influence of these factors on the ambient VOCs level can be reflected by the patterns of seasonal variation and diurnal variation. For Ji'nan, the level of VOCs at urban and industrial sites was mainly affected by local fresh emissions, while at background site was mainly influenced by regional transport.

### 3.3. Impact of petrochemical industry on VOCs

Diagnose indicators of T/B (toluene/benzene) and X/E (*m/p*-xylene/ethylbenzene) ratios were calculated to evaluate the relative importance of different VOCs emission sources (Fig. 5). A lower X/E ratio usually indicates an aging air mass (i.e., a large influence of regional transport) (Han et al., 2017; Phuc and Oanh, 2018). For T/B ratios, a value in the range of 0.2–0.4, 0.9–1.5, and >1.5 usually indicates a large influence of combustion source, vehicle exhaust, and industrial activity, respectively (Zhang et al., 2016). The lowest X/E ratios were observed at background site (1.9 ± 0.4), followed by two urban sites (QS: 2.1 ± 1.1; EMCS: 2.1 ± 0.8) and industrial site (3.2 ± 1.3). The highest T/B ratios were observed at industrial site (2.1 ± 10.5) with 32.7 % of the data larger than 1.5. Followed were those observed at urban sites (QS: 0.9 ± 2.6; EMCS: 1.1 ± 2.9), with 19.8 % (19.9 %) and 6.1 % (8.3 %) of the data in the range of 0.9–1.5 and >1.5 at QS (EMCS). The lowest T/B ratios were observed at background site (0.8 ± 1.1), with 17.1 % and 4.8 % of the data in the range of 0.9–1.5 and >1.5. The diagnose indicators indicate the significant impact of fresh emissions on VOCs at urban and industrial sites but of regional transport on VOCs at background site. The distribution of T/B ratios elucidates an important contribution of petrochemical industry to VOCs in Ji'nan (rather than a local scale).

Petrochemical industry is certainly an important VOCs emission source (Dai et al., 2022), not only in Ji'nan but also in many other cities such as Beijing (Song et al., 2007), Shanghai (Cai et al., 2010), Langfang (Song et al., 2019), Guangzhou (Yuan et al., 2013), and Houston (Ryerson et al., 2003). To obtain the detailed VOCs emission profile from petrochemical industry, source data were selected according to the following criteria: (a) T/B ratio larger than 4.2 (Barletta et al., 2008; Zhang et al., 2016); (b) X/E ratio larger than 2.0; (c) exclusion of data in the rush hours and during periods with intense photochemistry; (d) observation data at industrial site. The aim was to reduce the interferences introduced by vehicle exhaust and to assure that the selected data were mainly subject to the influence of petrochemical industry. The VOCs emission profiles were derived by subtracting the regional background from the source data, and the regional background level was calculated as the average of the lowest 10th percentile of data measured at background site (i.e., PML) (Chen et al., 2020). As shown in Fig. 6, light alkanes ($C_2$–$C_5$), aromatics, long-chain alkanes ($C_6$–$C_{12}$), alkenes, and alkynes accounted for 50.0 %, 19.5 %, 12.6 %, 10.9 %,

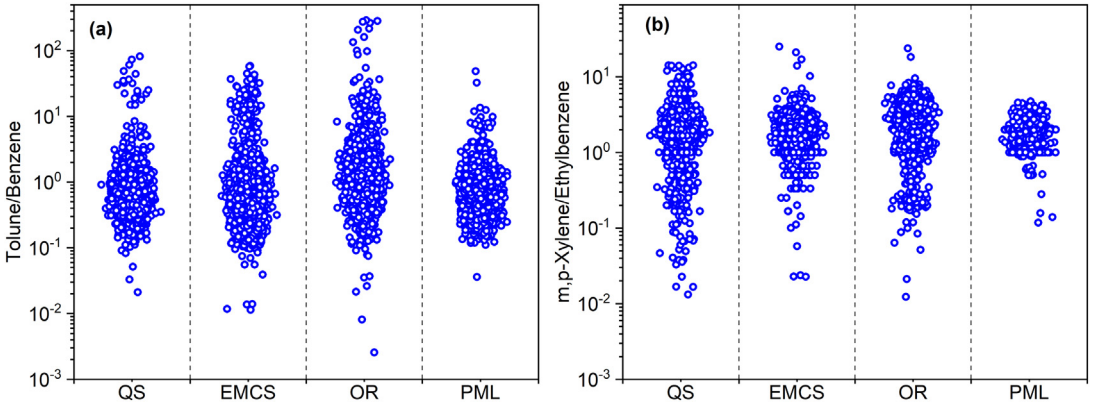


**Fig. 5.** The ratios of (a) toluene/benzene and (b) *m/p*-xylene/ethylbenzene at individual sites (i.e., QS, EMCS, OR, and PML).

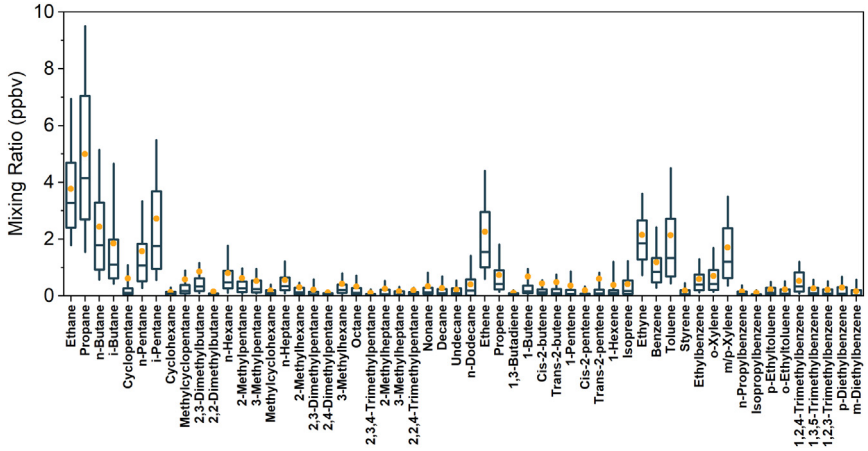


**Fig. 6.** VOCs emission profile from petrochemical industry obtained based on measured data at OR. The box plot provides the 10th, 25th, 50th, 75th, and 90th percentiles of the data, and the yellow circle represents the average. Detailed method for the calculation of VOCs emission profile was documented in Section 3.3.

and 7.0 % of the total measured species, respectively. On species level, propane (15.7 %), ethane (12.4 %), ethyne (7.0 %), *n*-butane (6.7 %), *i*-pentane (6.6 %), ethene (5.8 %), toluene (5.0 %), *m/p*-xylene (4.6 %), *i*-butane (4.2 %), and *n*-pentane (4.0 %) were identified as the top 10 abundant species. The emission profile of VOCs from petrochemical industry obtained in this study was generally consistent to that in Shanghai (Gao et al., 2022), but was slightly different from that in Izmir (Turkey) (Cetin et al., 2003) and Hangzhou (Mo et al., 2015), which found a huge impact of petrochemical activity on alkanes and alkenes (mainly propene and ethene). The difference should be related to the dominance of different petrochemical industrial processes (see below).

To refine the impact of different petrochemical industrial processes, the PMF model was applied to determine major VOCs emission sources and their respective contributions. Totally six factors were resolved in Ji'nan, i.e., refining process, combustion source, solvent usage, biogenic emission, vehicle exhaust, and O&G (oil and gas) usage (see SI for the detailed information of source profile). Three points are noteworthy in Fig. 7. First, the contributions of refining process and solvent usage were resolved at all sites, again demonstrating the impact of petrochemical industry on urban air quality in Ji'nan. Second, different species would be emitted during different petrochemical industrial processes (Li et al., 2019a, 2019b). Alkanes and alkenes dominated the emissions during refining process, while aromatics dominated the emissions during solvent usage process. Third, petrochemical industry (29.0 %–40.5 %), combustion (25.0 %–50.4 %), and vehicle exhaust (17.1 %–25.3 %) were identified as major VOCs sources in Ji'nan with concentration-based results. The impact of petrochemical industry on VOCs declined along with increasing distance to the industrial site (also demonstrated by diagnose indicators). The reactivity-based results are not that consistent with those obtained based on VOCs concentrations. The contributions of petrochemical industry to VOCs were enhanced based on $L_{OH}$ (from 29.0 %–40.5 % to 28.0 %–51.3 %), while those of vehicle exhaust levelled off (from 17.1 %–25.3 % to 17.1 %–24.3 %) and those of combustion were largely lowered (from 25.0 %–50.4 % to 12.5 %–27.5 %).

Based on observational evidence and PMF model analysis, we examined the impact of petrochemical industry and its major processes on VOCs. The intensive emissions of VOCs from petrochemical industry went far beyond industrial areas and exerted significant impact on urban air quality in Ji'nan. During the petrochemical industrial process, refining process would exert a huge impact on alkanes and alkenes, while solvent usage would exert a huge impact on aromatics. More studies should be conducted to further refine the impact of different petrochemical industrial processes.

### *3.4. Comparison of $O_3$ formation mechanisms between industrial and other sites*

An OBM coupled with RACM2 was applied to diagnose $O_3$ formation mechanisms and to examine the impact of petrochemical industry on $O_3$ formation. The chemical production of $O_3$ was the most intense at industrial site (29.9–49.8 ppbv/h; 9:00–15:00 LT), followed by urban sites (QS: 19.2–38.7 ppbv/h; EMCS: 18.1–35.0 ppbv/h) and background site (0.9–9.5 ppbv/h) (Fig. S8). There is a strong in-situ $O_3$ production capacity in Ji'nan, especially at industrial site, which was comparable to or even higher than those derived from megacities such as Beijing (Jia et al., 2023) and Shanghai (Zhang et al., 2021a). The chemical production of $O_3$ was the most intense in summer (9.5–49.8 ppbv/h), followed by spring (2.3–41.5 ppbv/h) and autumn (0.9–29.9 ppbv/h). Such seasonal variation pattern is generally consistent to that of observed $O_3$ concentrations (Fig. S1). An interesting phenomenon is the fast $O_3$ production at industrial

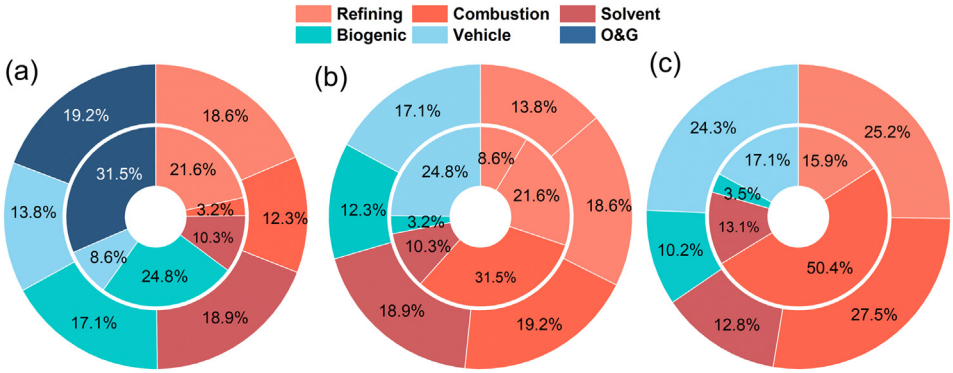


**Fig. 7.** Contributions of major emission sources to ambient VOCs observed at (a) urban, (b) industrial, and (c) background sites in Ji'nan based on the PMF results. The outer and inner rings were for $L_{OH}$-based and concentration-based results, respectively.

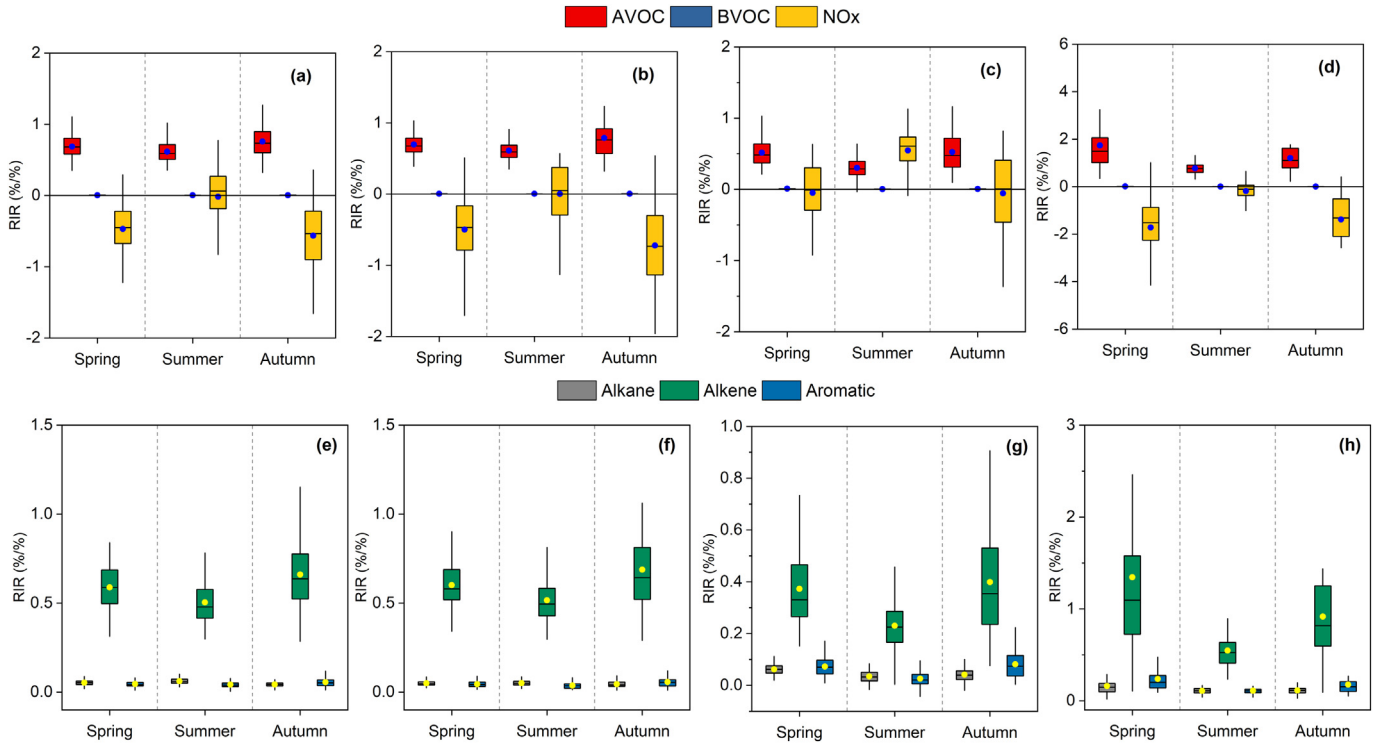


**Fig. 8.** Modeled RIRs for major $O_3$ precursor groups (i.e., AVOCs, BVOCs, and $NO_x$) and major AVOCs groups (i.e., alkane, alkene, and aromatic) at urban (QS: (a) & (e); EMCS: (b) & (f)), industrial ((c) & (g)), and background ((d) and (h)) sites. RIR: relative incremental reactivity; AVOCs: anthropogenic VOCs; BVOCs: biogenic VOCs.

site in the morning, which has been also found in an oil production region in northern China (Chen et al., 2020) and should be driven by the intensive VOCs emissions from petrochemical industry.

Several spatial and temporal features were shown in the $O_3$ formation regimes (Fig. 8). The urban and background sites persist in a VOCs-limited $O_3$ formation regime and AVOCs showed the largest relative incremental reactivity (RIR) values (urban: 0.61–0.79; background: 0.82–1.39) (see SI for the calculation of RIR). Among major AVOCs groups, alkenes showed the largest RIR values (urban: 0.51–0.69; background: 0.59–1.03). A 20 % reduction in $NO_x$ emissions would aggravate $O_3$ pollution (RIR: -0.72–0.00 and -1.44 to -0.52 at urban and background sites, respectively). The VOCs-limited $O_3$ formation regime at background site in this study is different from that mentioned in previous studies (generally $NO_x$-limited) (Wang et al., 2022), which should be attributed to the low VOCs/$NO_x$ ratios (0.91) at PML (even lower than urban Guangzhou (Zhang et al., 2021b)). We also found similar case at the other background sites (He et al., 2019; Su et al., 2018). Similarly, the industrial site was in a VOCs-limited $O_3$ formation regime in spring and autumn, with AVOCs showing the highest RIR values (spring: 0.52; autumn: 0.52). In contrast, the industrial site shifted to a $NO_x$-limited $O_3$ formation regime in summer ($NO_x$: 0.55; AVOCs: 0.30). In all three seasons, a higher sensitivity to $NO_x$ was determined at industrial site compared to urban and background sites. The RIRs for BVOCs (0.00–0.04) were relatively small. These spatial and temporal features in the $O_3$ formation regimes were determined by the relative abundance of $NO_x$ and VOCs. As shown in Table S1, the average VOCs/$NO_x$ ratio at urban and background sites was largely lower than that at industrial site. And at industrial site, the average VOCs/$NO_x$ ratio was higher in summer than in spring and autumn. The relatively high VOCs abundance tends to accelerate radical recycling, which can lead to $NO_x$ cycle being the key process to limit $O_3$ production (i.e., $NO_x$-limited).

We then determined the impact of emission reduction from major sources (i.e., refining process, combustion source, solvent usage, vehicle

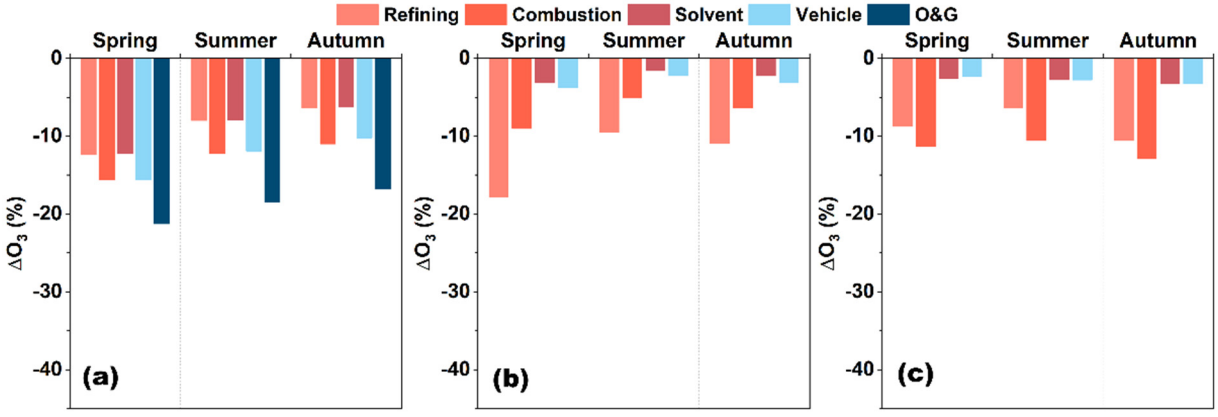


**Fig. 9.** Modeled $O_3$ change with 50 % reduction from major anthropogenic emission sectors (i.e., refining process, combustion source, solvent usage, vehicle exhaust, and O&G usage) at (a) urban, (b) industrial, and (c) background sites.

exhaust, and O&G usage) on $O_3$ production by combining PMF results and OBM analysis (Fig. 9). With a reduction ratio of 50 %, O&G usage, petrochemical industry, and combustion source were identified as the key emission sectors at urban (16.8 %–21.3 %), industrial (9.5 %–17.9 %), and background sites (10.5 %–12.9 %), respectively. The effects of AVOCs emission reduction from vehicle exhaust (4.6 %–7.6 %) were relatively small. For the whole Ji'nan city, the control of AVOCs emissions from petrochemical industry would be the most effective way to alleviate $O_3$ pollution (urban: 12.6 %–24.6 %; industrial: 9.5 %–21.0 %; background: 9.2 %–13.4 %). We also performed analyses with 100 % reductions and the key emission sectors remain unchanged (Fig. S9). Specific to process level, the control of AVOCs emissions from refining process (urban: 6.4 %–12.4 %; industrial: 9.5 %–17.9 %; background: 6.4 %–10.6 %) would be more effective than solvent usage (urban: 6.2 %–12.2 %; industrial: 1.6 %–3.1 %; background: 2.6 %–3.3 %).

### 3.5. Implications for control policy against $O_3$ pollution

As mentioned above, AVOCs played an important role in the chemical production of $O_3$. To aid in the development and refinement of control strategies against $O_3$ pollution, the non-linear dependence of $O_3$ on $NO_x$ and AVOCs was examined in detail at industrial and urban sites with strong in-situ $O_3$ production capacity. The model-simulated MDA8 $O_3$ concentrations under base scenarios were 83 ppbv at QS, 85 ppbv at EMCS, and 91 ppbv at OR (Fig. 10), which were comparable to observation data (QS: 88 ppbv; EMCS: 94 ppbv; OR: 91 ppbv). The good consistency indicates that the model could well reproduce the formation of $O_3$ pollution.

As shown in Fig. 10, the industrial and urban sites are clearly under VOCs-limited $O_3$ formation regimes during the $O_3$ non-attainment days. Decrease in AVOCs concentrations would effectively alleviate $O_3$ pollution during a short-time period, while a small decrease in $NO_x$ concentrations would aggravate $O_3$ pollution. The attainment of $O_3$ concentration (MDA8 $O_3$ < 75 ppbv) can be achieved if the $NO_x$ concentration is reduced by −95 % and −90 %, or the AVOCs concentration is reduced by −10 % and −15 % at urban and industrial sites, respectively. It is noted that the effect of 100 % reduction in $NO_x$ on alleviating $O_3$ pollution was superior than that of 100 % reduction in AVOCs. Quantitatively, the MDA8 $O_3$ concentrations in urban Ji'nan would be reduced by −90 % (for urban sites) and by −99 % (for industrial site) with 100 % $NO_x$ reduction, but merely by −76 % (for urban sites) and by −81 % (for industrial site) with 100 % AVOCs reduction. This is mainly attributed to the BVOCs emission, which could lessen the benefit resulted from large decrease in AVOCs concentration. By taking BVOCs emission into account (beyond control efforts), large decrease in $NO_x$ concentration is a more controllable way to mitigate $O_3$ pollution in the long run. To shift the $O_3$ formation regime from VOCs-limited to mix-limited (by $NO_x$ and VOCs), the $NO_x$ concentration needs to be reduced by 60 % and 50 % at urban and industrial sites, respectively (see the black solid line in Fig. 10). During this process, collaborative control of $NO_x$ and AVOCs with $\triangle$AVOCs/$\triangle NO_x$ > 0.79 (for urban sites) and $\triangle$AVOCs/$\triangle NO_x$ > 0.66 (for industrial site) should be implemented to avoid exacerbation of $O_3$ pollution in Ji'nan (see the black dashed line in Fig. 10).

The above strategy focusing on collaborative simultaneous AVOCs and $NO_x$ reduction and large $NO_x$ reduction was recommended as a future step against $O_3$ pollution, not only in Ji'nan but also in many Chinese metropolitan areas which are currently under VOCs-limited $O_3$ formation regimes (Wang et al., 2022). Note that the EKMA curve and science-based AVOCs/$NO_x$ reduction ratio would vary between different cities (or different periods for a particular city) (Ou et al., 2016; Zhao et al., 2022), owing to the changes in local environmental conditions such as VOCs/$NO_x$ ratio, VOCs chemical composition, and meteorological condition. Thus, the science-based AVOCs/$NO_x$ reduction ratio needs to be examined on a regular basis based on changes in local environmental conditions.

## 4. Conclusions

Two-year continuous measurements were conducted at urban, background, and industrial areas in Ji'nan, eastern China. The data were analyzed to examine the VOCs pollution characteristics, sources, and impact on $O_3$ pollution. The major findings are summarized as follows.

On the spatial and temporal distribution of VOCs: Higher VOCs concentrations and an increasingly importance of aromatics were detected at industrial site than at urban and background sites, owing to intensive emissions from petrochemical industry. Temporally, the VOCs concentrations showed well-defined seasonal variation (peak in autumn or winter) and diurnal variation (with two peaks in the rush hours) patterns at industrial and urban sites, contrasting to the flat pattern shown by VOCs concentrations at background site.

On the impact of petrochemical industry on VOCs: The intensive VOCs emissions from petrochemical industry went far beyond industrial areas and exerted significant impact on urban air quality in Ji'nan, as indicated by both diagnose indicators and PMF model analysis. During the petrochemical industrial process, refining would exert a huge impact on alkanes (propane, ethane, *n*-butane, *i*-pentane, *i*-butane, and *n*-pentane) and alkenes (ethene), while solvent usage would exert a huge impact on aromatics (toluene and *m/p*-xylene).

On the $O_3$ formation mechanisms: There is a strong in-situ $O_3$ production capacity in Ji'nan. The urban and background sites persist in a VOCs-limited $O_3$ formation regime with alkenes being the key precursors. The industrial site was in a VOCs-limited, $NO_x$-limited, and VOCs-limited $O_3$ formation regime in spring, summer, and autumn, respectively, with alkenes being the key VOCs precursors. The reduction of VOCs emissions from petrochemical industry would be an effective way to alleviate $O_3$ pollution in Ji'nan.

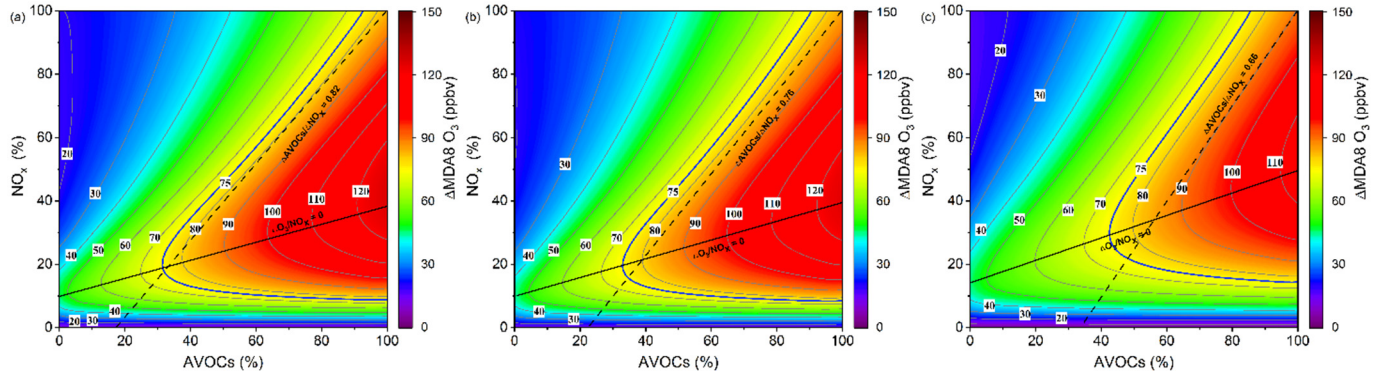


**Fig. 10.** Isopleths of the modeled MDA8 $O_3$ concentrations as a function of *X* folds the base concentrations of AVOCs and $NO_x$ at (a) QS, (b) EMCS, and (c) OR. The black dashed line represents the fitting line for a base case with an AVOCs/$NO_x$ reduction ratio of 0.82, 0.76, and 0.66 [i.e., percentage change in concentration (ppbv)/percentage change in concentration (ppbv)], which exerts nearly zero effect on $O_3$ production. The black solid line represents the boundary between the VOCs-limited and mix-limited $O_3$ formation regime.

## CRediT authorship contribution statement

**Jiangshan Mu:** Conceptualization, Data curation, Formal analysis, Writing – original draft. **Yingnan Zhang:** Conceptualization, Formal analysis, Writing – original draft. **Zhiyong Xia:** Investigation, Resources. **Guolan Fan:** Investigation, Resources. **Min Zhao:** Formal analysis. **Xiaoyan Sun:** Investigation, Resources. **Yuhong Liu:** Resources. **Tianshu Chen:** Conceptualization, Resources. **Hengqing Shen:** Conceptualization. **Zhanchao Zhang:** Investigation, Resources. **Huaicheng Zhang:** Investigation, Resources. **Guang Pan:** Investigation, Resources. **Wenxing Wang:** Supervision, Writing – review & editing. **Likun Xue:** Conceptualization, Supervision, Project administration, Funding acquisition, Writing – review & editing.

## Data availability

Data will be made available on request.

## Declaration of competing interest

The authors declare that they have no known competing financial interests or personal relationships that could have appeared to influence the work reported in this paper.

## Acknowledgement

We appreciate the Regional Atmospheric Chemistry Mechanism development groups for provision of the mechanisms. This work was funded by the National Natural Science Foundation of China (41922051 and 42061160478), the Shandong Provincial Science Foundation for Distinguished Young Scholars (grant no. ZR2019JQ09), and the National Research Program for Key Issues in Air Pollution Control (DQGG202118).

## Appendix A. Supplementary data

Supplementary data to this article can be found online at https://doi.org/10.1016/j.scitotenv.2022.159951.

## References

An, J., Zhu, B., Wang, H., Li, Y., Lin, X., Yang, H., 2014. Characteristics and source apportionment of VOCs measured in an industrial area of Nanjing, Yangtze River Delta,China. Atmos. Environ. 97, 206–214.

An, J., Wang, J., Zhang, Y., Zhu, B., 2017. Source apportionment of volatile organic compounds in an urban environment at the Yangtze River Delta, China. Arch. Environ. Contam. Toxicol. 72, 335–348.

Atkinson, R., 2000. Atmospheric chemistry of VOCs and NOx. Atmos. Environ. 34, 2063–2101.

Barletta, B., Meinardi, S., Simpson, I.J., Zou, S., Rowland, F.S., Blake, D.R., 2008. Ambient mixing ratios of nonmethane hydrocarbons (NMHCs) in two major urban centers of the Pearl River Delta (PRD) region: Guangzhou and Dongguan. Atmos. Environ. 42, 4393–4408.

Cai, C., Geng, F., Tie, X., Yu, Q., An, J., 2010. Characteristics and source apportionment of VOCs measured in Shanghai,China. Atmos. Environ. 44, 5005–5014.

Cetin, E., Odabasi, M., Seyfioglu, R., 2003. Ambient volatile organic compound (VOC) concentrations around a petrochemical complex and a petroleum refinery. Sci. Total Environ. 312, 103–112.

Chen, T., Xue, L., Zheng, P., Zhang, Y., Liu, Y., Sun, J., et al., 2020. Volatile organic compounds and ozone air pollution in an oil production region in northern China. Atmos. Chem. Phys. 20, 7069–7086.

CNEMC, 2018. Technical Specifications for Operations and Quality Control of Ambient Air Quality Continuous Automated Monitoring System for SO2, NO2, O3 and CO (in Chinese).

Cui, L., Wu, D., Wang, S., Xu, Q., Hu, R., Hao, J., 2022. Measurement report: ambient volatile organic compound (VOC) pollution in urban Beijing: characteristics, sources, and implications for pollution control. Atmos. Chem. Phys. 22 (18), 11931–11944.

Dai, L., Meng, J., Zhao, X., Li, Q., Shi, B., Wu, M., et al., 2022. High-spatial-resolution VOCs emission from the petrochemical industries and its differential regional effect on soil in typical economic zones of China. Sci. Total Environ. 827, 154318.

Debevec, C., Sauvage, S., Gros, V., Salameh, T., Sciare, J., Dulac, F., et al., 2021. Seasonal variation and origins of volatile organic compounds observed during 2 years at a western Mediterranean remote background site (Ersa, Cape Corsica). Atmos. Chem. Phys. 21, 1449–1484.

EPA, 2014. Positive Matrix Factorization (PMF) 5.0-Fundamentals and User Guide. US Environmental Protection Agency, Washington DC.

Fares, S., Schnitzhofer, R., Jiang, X., Guenther, A., Hansel, A., Loreto, F., 2013. Observations of diurnal to weekly variations of monoterpene-dominated fluxes of volatile organic compounds from Mediterranean forests: implications for regional modeling. Environ.Sci. Technol. 47, 11073–11082.

Gao, S., Zhang, Z., Wang, Q., Ma, Y., Wu, S., Cui, H., et al., 2022. Emissions and health risk assessment of process-based volatile organic compounds of a representative petrochemical enterprise in East China. Air Qual.Atmo.Health 15 (6), 1095–1109.

Gross, A., Stockwell, W.R., 2003. Comparison of the EMEP, RADM2 and RACM mechanisms. J. Atmos. Chem. 44, 151–170.

Guan, Y., Wang, L., Wang, S., Zhang, Y., Xiao, J., Wang, X., et al., 2020. Temporal variations and source apportionment of volatile organic compounds at an urban site in Shijiazhuang,China. J. Environ. Sci. 97, 25–34.

Guo, H., Ling, Z., Cheng, H., Simpson, I., Lyu, X., Wang, X., et al., 2017. Tropospheric volatile organic compounds in China. Sci. Total Environ. 574, 1021–1043.

Han, D., Wang, Z., Cheng, J., Wang, Q., Chen, X., Wang, H., 2017. Volatile organic compounds (VOCs) during non-haze and haze days in Shanghai: characterization and secondary organic aerosol (SOA) formation. Environ. Sci. Pollut. Res. 24, 18619–18629.

Han, D., Gao, S., Fu, Q., Cheng, J., Chen, X., Xu, H., et al., 2018. Do volatile organic compounds (VOCs) emitted from petrochemical industries affect regional PM2.5? Atmos. Res. 209, 123–130.

He, Z., Wang, X., Ling, Z., Zhao, J., Guo, H., Shao, M., et al., 2019. Contributions of different anthropogenic volatile organic compound sources to ozone formation at a receptor site in the Pearl River Delta region and its policy implications. Atmos. Chem. Phys. 19 (13), 8801–8816.

Hoshi, J.-y., Amano, S., Sasaki, Y., Korenaga, T., 2008. Investigation and estimation of emission sources of 54 volatile organic compounds in ambient air in Tokyo. Atmos. Environ. 42, 2383–2393.

Jia, C., Tong, S., Zhang, X., Li, F., Zhang, W., Li, W., et al., 2023. Atmospheric oxidizing capacity in autumn Beijing: analysis of the O3 and PM2.5 episodes based on observation-based model. J. Environ. Sci. 124, 557–569.

Li, G., Wei, W., Wei, F., Cheng, S., Wen, W., Wang, G., 2014. Diurnal variations of ozone and its precursors and ozone formation potential of VOCs at the boundary of a coking plant during summer and autumn. J. Environ. Eng. 8, 130–1138.

Li, M., Liu, H., Geng, G., Hong, C., Liu, F., Song, Y., et al., 2017. Anthropogenic emission inventories in China: a review. Natl. Sci. Rev. 4, 834–866.

Li, M., Zhang, Q., Zheng, B., Tong, D., Lei, Y., Liu, F., et al., 2019. Persistent growth of anthropogenic non-methane volatile organic compound (NMVOC) emissions in China during 1990–2017: drivers, speciation and ozone formation potential. Atmos. Chem. Phys. 19, 8897–8913.

Li, Q., Su, G., Li, C., Wang, M., Tan, L., Gao, L., et al., 2019. Emission profiles, ozone formation potential and health-risk assessment of volatile organic compounds in rubber footwear industries in China. J. Hazard. Mater. 375, 52–60.

Li, J., Li, H., He, Q., Guo, L., Zhang, H., Yang, G., et al., 2020. Characteristics, sources and regional inter-transport of ambient volatile organic compounds in a city located downwind of several large coke production bases in China. Atmos. Environ. 233, 117573.

Li, Q., Su, G., Li, C., Liu, P., Zhao, X., Zhang, C., et al., 2020. An investigation into the role of VOCs in SOA and ozone production in Beijing,China. Sci. Total Environ. 720, 137536.

Liu, Z., Li, N., Wang, N., 2016. Characterization and source identification of ambient VOCs in Jinan, China. Air Qual.Atmos.Health 9, 285–291.

Liu, Y., Wang, H., Jing, S., Gao, Y., Peng, Y., Lou, S., et al., 2019. Characteristics and sources of volatile organic compounds (VOCs) in Shanghai during summer: implications of regional transport. Atmos. Environ. 215, 116902.

Liu, Y., Song, M., Liu, X., Zhang, Y., Hui, L., Kong, L., et al., 2020. Characterization and sources of volatile organic compounds (VOCs) and their related changes during ozone pollution days in 2016 in Beijing,China. Environ. Pollut. 257, 113599.

Liu, Y., Kong, L., Liu, X., Zhang, Y., Li, C., Zhang, Y., et al., 2021a. Characteristics, secondary transformation, and health risk assessment of ambient volatile organic compounds (VOCs) in urban Beijing,China. Atmos. Pollut. Res. 12, 33–46.

Liu, Y., Shen, H., Mu, J., Li, H., Chen, T., Yang, J., et al., 2021b. Formation of peroxyacetyl nitrate (PAN) and its impact on ozone production in the coastal atmosphere of Qingdao, North China. Sci. Total Environ. 778, 146265.

MEEPRC, 2013. HJ644-2013 Ambient Air - Determination of Volatile Organic Compounds -Sorbent Adsorption and Thermal Desorption/Gas Chromatography Mass Spectrometry Method (in Chinese). . https://www.mee.gov.cn/ywgz/fgbz/bz/bzwb/jcffbz/201302/t20130222_248384.shtml.

Mo, Z., Shao, M., Lu, S., Qu, H., Zhou, M., Sun, J., et al., 2015. Process-specific emission characteristics of volatile organic compounds (VOCs) from petrochemical facilities in the Yangtze River Delta. Sci. Total Environ. 533, 422–431.

Mozaffar, A., Zhang, Y.-L., 2020. Atmospheric volatile organic compounds (VOCs) in China: a review. Curr.Pollut.Rep. 6, 250–263.

Ou, J., Yuan, Z., Zheng, J., Huang, Z., Shao, M., Li, Z., et al., 2016. Ambient ozone control in a photochemically active region: short-term despiking or long-term attainment? Environ. Sci.Technol. 50 (11), 5720–5728.

Paatero, P., 1997. Least squares formulation of robust non-negative factor analysis. Chemom. Intell. Lab. Syst. 37, 23–35.

Paatero, P., Tapper, U., 1994. Positive matrix factorization: a non-negative factor model with optimal utilization of error estimates of data values. Environmetrics 5, 111–126.

Phuc, N.H., Oanh, N.T.K., 2018. Determining factors for levels of volatile organic compounds measured in different microenvironments of a heavy traffic urban area. Sci. Total Environ. 627, 290–303.

Rao, P., Ansari, M., Gavane, A., Pandit, V., Nema, P., Devotta, S., 2007. Seasonal variation of toxic benzene emissions in petroleum refinery. Environ. Monit. Assess. 128, 323–328.

Rovira, J., Nadal, M., Schuhmacher, M., Domingo, J.L., 2021. Environmental impact and human health risks of air pollutants near a large chemical/petrochemical complex: case study in Tarragona,Spain. Sci. Total Environ. 787, 147550.

Ryerson, T., Trainer, M., Angevine, W., Brock, C., Dissly, R., Fehsenfeld, F., et al., 2003. Effect of petrochemical industrial emissions of reactive alkenes and NOx on tropospheric ozone formation in Houston, Texas. J. Geophys. Res. Atmos. 108.

Seinfeld, J.H., Pandis, S.N., 1998. From air pollution to climate change. Atmos. Chem. Phys. 1326.

Sillman, S., 1999. The relation between ozone, NOx and hydrocarbons in urban and polluted rural environments. Atmos. Environ. 33, 1821–1845.

Song, Y., Shao, M., Liu, Y., Lu, S., Kuster, W., Goldan, P., et al., 2007. Source apportionment of ambient volatile organic compounds in Beijing. Environ.Sci.Technol. 41, 4348–4353.

Song, C., Liu, B., Dai, Q., Li, H., Mao, H., 2019. Temperature dependence and source apportionment of volatile organic compounds (VOCs) at an urban site on the North China Plain. Atmos. Environ. 207, 167–181.

Stockwell, W.R., Kirchner, F., Kuhn, M., Seefeld, S., 1997. A new mechanism for regional atmospheric chemistry modeling. J.Geophys.Res.Atmos. 102, 25847–25879.

Su, R., Lu, K., Yu, J., Tan, Z., Jiang, M., Li, J., et al., 2018. Exploration of the formation mechanism and source attribution of ambient ozone in Chongqing with an observation-based model. Sci.China Earth Sci. 61 (1), 23–32.

Sun, L., Xue, L., Wang, T., Gao, J., Ding, A., Cooper, O.R., et al., 2016. Significant increase of summertime ozone at mount tai in Central Eastern China. Atmos. Chem. Phys. 16, 10637–10650.

Von Schneidemesser, E., Monks, P.S., Plass-Duelmer, C., 2010. Global comparison of VOC and CO observations in urban areas. Atmos. Environ. 44, 5053–5064.

Wang, M., Zeng, L., Lu, S., Shao, M., Liu, X., Yu, X., et al., 2014. Development and validation of a cryogen-free automatic gas chromatograph system (GC-MS/FID) for online measurements of volatile organic compounds. Anal. Methods 6, 9424–9434.

Wang, T., Xue, L., Brimblecombe, P., Lam, Y.F., Li, L., Zhang, L., 2017. Ozone pollution in China: a review of concentrations, meteorological influences, chemical precursors, and effects. Sci. Total Environ. 575, 1582–1596.

Wang, N., Lyu, X., Deng, X., Huang, X., Jiang, F., Ding, A., 2019. Aggravating O3 pollution due to NOx emission control in eastern China. Sci. Total Environ. 677, 732–744.

Wang, Z., Wang, H., Zhang, L., Guo, J., Li, Z., Wu, K., et al., 2021. Characteristics of volatile organic compounds (VOCs) based on multisite observations in Hebei province in the warm season in 2019. Atmos. Environ. 256, 118435.

Wang, T., Xue, L., Feng, Z., Dai, J., Zhang, Y., Tan, Y., 2022. Ground-level ozone pollution in China: a synthesis of recent findings on influencing factors and impacts. Environ. Res. Lett. 17, 063003.

Warneke, C., De Gouw, J.A., Holloway, J.S., Peischl, J., Ryerson, T.B., Atlas, E., et al., 2012. Multiyear trends in volatile organic compounds in Los Angeles, California: five decades of decreasing emissions. J. Geophys. Res. Atmos. 117.

Wei, W., Chen, S., Wang, Y., Chen, L., Wang, X., Cheng, S., 2022. The impacts of VOCs on PM2.5 increasing via their chemical losses estimates: a case study in a typical industrial city of China. Atmos. Environ. 273, 118978.

Wu, R., Xie, S., 2017. Spatial distribution of ozone formation in China derived from emissions of speciated volatile organic compounds. Environ.Sci.Technol. 51, 2574–2583.

Wu, F., Yu, Y., Sun, J., Zhang, J., Wang, J., Tang, G., et al., 2016. Characteristics, source apportionment and reactivity of ambient volatile organic compounds at Dinghu Mountain in Guangdong Province,China. Sci. Total Environ. 548, 347–359.

Xue, L., Wang, T., Gao, J., Ding, A., Zhou, X., Blake, D., et al., 2014. Ground-level ozone in four Chinese cities: precursors, regional transport and heterogeneous processes. Atmos. Chem. Phys. 14, 13175–13188.

Yuan, Z., Zhong, L., Lau, A.K.H., Yu, J.Z., Louie, P.K., 2013. Volatile organic compounds in the Pearl River Delta: identification of source regions and recommendations for emission-oriented monitoring strategies. Atmos. Environ. 76, 162–172.

Zhang, Z., Zhang, Y., Wang, X., Lü, S., Huang, Z., Huang, X., et al., 2016. Spatiotemporal patterns and source implications of aromatic hydrocarbons at six rural sites across China's developed coastal regions. J.Geophys.Res.Atmos. 121, 6669–6687.

Zhang, K., Huang, L., Li, Q., Huo, J., Duan, Y., Wang, Y., et al., 2021a. Explicit modeling of isoprene chemical processing in polluted air masses in suburban areas of the Yangtze River Delta region: radical cycling and formation of ozone and formaldehyde. Atmos. Chem. Phys. 21, 5905–5917.

Zhang, Y., Xue, L., Carter, W.P., Pei, C., Chen, T., Mu, J., et al., 2021b. Development of ozone reactivity scales for volatile organic compounds in a Chinese megacity. Atmos. Chem. Phys. 21, 11053–11068.

Zhao, M., Zhang, Y., Pei, C., Chen, T., Mu, J., Liu, Y., et al., 2022. Worsening ozone air pollution with reduced NOx and VOCs in the Pearl River Delta region in autumn 2019: implications for national control policy in China. J. Environ. Manag. 324, 116327.

Zong, R., Xue, L., Wang, T., Wang, W., 2018. Inter-comparison of the regional atmospheric chemistry mechanism (RACM2) and master chemical mechanism (MCM) on the simulation of acetaldehyde. Atmos. Environ. 186, 144–149.